ATLAS NOTE

ATLAS-CONF-2013-026

March 8, 2013

Search for Supersymmetry in Events with Large Missing Transverse Momentum, Jets, and at Least One Tau Lepton in 21 fb^{-1} of $\sqrt{s}$ = 8 TeV Proton-Proton Collision Data with the ATLAS Detector

The ATLAS Collaboration

Abstract

A search for supersymmetry in events with large missing transverse momentum, jets, at least one hadronically decaying τ lepton and zero additional light leptons (e/μ), has been performed using 20.7 fb^{-1} of proton-proton collision data at $\sqrt{s}$ = 8 TeV recorded with the ATLAS detector at the Large Hadron Collider. No excess above the Standard Model background expectation is observed and a 95% confidence level visible cross section upper limit for new phenomena is set. In the framework of minimal gauge-mediated SUSY breaking models, exclusion limits on the breaking scale Λ are set at 54 TeV, independently of $\tan\beta$. Exclusion limits are derived also for an mSUGRA/CMSSM model, for which the parameters are chosen in such a way that the Higgs mass is compatible with the recent discovery of a Higgs boson-like particle at the LHC. A further interpretation is presented in a framework of natural gauge mediation in which the gluino is assumed to be the only light coloured sparticle and decays in τ-enriched final states. Gluino masses below 1.14 TeV are excluded in this hypothesis.

ATLAS-CONF-2013-026
11 March 2013

1 Introduction

This note reports on the search for supersymmetry (SUSY) [1–9] in events with large missing transverse momentum, jets and at least one hadronically decaying τ lepton. Two distinct decay topologies with either one τ lepton or at least two τ leptons in the final state have been studied. The analysis has been performed using 20.7 fb^{-1} of proton-proton (pp) collision data at $\sqrt{s} = 8$ TeV recorded with the ATLAS detector at the Large Hadron Collider (LHC) in the 2012 run. The results are interpreted in the context of a minimal gauge-mediated supersymmetry breaking (GMSB) model [10–15], an mSUGRA/CMSSM [16–21] model and in a natural gauge mediation framework (nGM) [22].

SUSY introduces a symmetry between fermions and bosons, resulting in a SUSY partner particle (sparticle) for each Standard Model (SM) particle, with identical mass and quantum numbers except a difference by half a unit of spin. As none of these sparticles have been observed with the same masses as their SM partners, SUSY must be a broken symmetry if realised in nature. Assuming R-parity conservation [23–27], sparticles are produced in pairs. These would then decay through cascades involving other sparticles until the lightest SUSY particle (LSP), which is stable, is produced.

Minimal GMSB models can be described by six parameters: the SUSY-breaking mass scale in the low-energy sector (Λ), the messenger mass (M_{mess}), the number of SU(5) messenger fields (N_5), the ratio of the vacuum expectation values of the two Higgs doublets ($\tan\beta$), the Higgs sector mass parameter (μ) and the scale factor for the gravitino mass (C_{grav}). For the analysis presented in this note, Λ and $\tan\beta$ are treated as free parameters, and the other parameters are fixed to the values already used in Ref. [28]: $M_{\text{mess}} = 250$ TeV, $N_5 = 3$, $\mu > 0$ and $C_{\text{grav}} = 1$. With this choice of parameters, the production of squark and/or gluino pairs is expected to dominate at the LHC. These sparticles will decay into the next-to-lightest SUSY particle (NLSP), which subsequently decays to the LSP. In gauge mediated models, the LSP is often a very light gravitino ($\tilde{G}$). Due to the very small LSP mass of O(keV), the NLSP is the only sparticle decaying to the LSP and this leads to experimental signatures which are largely determined by the nature of the NLSP. This can be either the lightest stau ($\tilde{\tau}$), a right handed slepton ($\tilde{\ell}$), the lightest neutralino ($\tilde{\chi}_1^0$), or a sneutrino ($\tilde{\nu}$), dominantly leading to final states containing τ leptons, light leptons ($\ell = e, \mu$), photons, or neutrinos, respectively. In the GMSB parameter space considered here, the $\tilde{\tau}$ is the NLSP for most of the parameter space at large values of $\tan\beta$, which leads to final states containing between two and four τ leptons. In the CoNLSP region, where the mass difference between the $\tilde{\tau}$ and the $\tilde{\ell}$ is smaller than the sum of the τ and light lepton masses, both the $\tilde{\tau}$ and the $\tilde{\ell}$ decay directly into the LSP and are therefore both NLSP.

In addition to the GMSB model, results are interpreted in an mSUGRA/CMSSM plane defined by five model parameters: the universal trilinear coupling ($A_0 = -2 \times m_0$), the universal scaler mass (m_0), the universal gaugino mass ($m_{1/2}$), the ratio of the vacuum expectation values of the two Higgs doublets ($\tan\beta$) and the sign of the Higgs sector mass parameter (μ). These were chosen such that across a large area of the plane the mSUGRA/CMSSM lightest Higgs boson mass is compatible with the recent discovery of a Higgs boson-like particle at the LHC [29, 30].

A richer phenomenology is obtained in the framework of general gauge mediation (GGM) [31]. Starting from GGM, it is possible to construct a natural gauge mediation (nGM) model by choosing values of the weak scale SUSY parameters that reduce the fine tuning in the Higgs sector. In the minimal supersymmetric model, this mostly depends on the μ-term and on sparticles with large couplings to the Higgs boson, namely the third generation sfermions, gluinos and electroweak gauginos. In the model considered here, it is assumed that the gluino is the only light coloured sparticle in order to set a conservative limit on the gluino mass. It is further assumed that $\mu << M_1, M_2$. Taking the weak scale supersymmetric parameters, all squark and slepton mass parameters are set to 2.5 TeV, except the lightest stau mass. $m_{\tilde{\tau}}$, which is assumed to be smaller in order to have a stau NLSP (this has no effect on the fine tuning). The bino (M_1) and wino (M_2) masses are also set to 2.5 TeV, while all trilinear coupling terms

Table 1: Dominant branching ratios for gluino decays in the nGM model, for models with $m_{\tilde{g}} > \approx 1$ TeV.

Process	Branching ratio (μ = 400 GeV)	Branching ratio (μ = 200 GeV)
$\tilde{g} \to t\bar{t}\,\tilde{\chi}_1^0$	$\approx 20\%$	$\approx 21\%$
$\tilde{g} \to t\bar{t}\,\tilde{\chi}_2^0$	$\approx 15\%$	$\approx 18\%$
$\tilde{g} \to \tilde{\chi}_1^+\, b\bar{t}$	$\approx 28\%$	$\approx 27\%$
$\tilde{g} \to \tilde{\chi}_1^-\, \bar{b}t$	$\approx 28\%$	$\approx 27\%$

are set to zero. This leaves the gluino mass M_3 and the stau mass $m_{\tilde{\tau}}$ as the only free parameters if μ is also fixed.

The value of μ is fixed to $\mu = 400$ GeV to ensure that strong production is the dominant process at the LHC. The exclusion reach of the analysis is only weakly dependent on μ over the range 200-400 GeV (provided the $\tilde{\tau}$ remains lighter), which is partly a consequence of the fact that two hard τ leptons are generated in every SUSY event from the decay $\tilde{\tau} \to \tau\tilde{G}$. The branching ratios for each dominant gluino decay mode are shown for $\mu = 200$ GeV and $\mu = 400$ GeV in Table 1, and show only a weak dependence on the value of μ.

Several decay modes are possible for the gluino:

1. $\tilde{g} \to g\tilde{\chi}_i^0 \to g\tau\,\tilde{\tau} \to g\tau\tau\tilde{G}$, with $i = 1, 2$
2. $\tilde{g} \to q\bar{q}\tilde{\chi}_i^0 \to q\bar{q}\tau\,\tilde{\tau} \to q\bar{q}\tau\tau\tilde{G}$, with $i = 1, 2$
3. $\tilde{g} \to qq'\tilde{\chi}_1^\pm \to qq'\tilde{\nu}_\tau\,\tilde{\tau} \to qq'\tilde{\nu}_\tau\tau\tilde{G}$

where q and $\bar{q}$ are almost exclusively quarks of heavy flavour (either top or bottom quarks). The first process proceeds through a squark-quark loop, and equal quantities of $\tilde{\chi}_1^0$ and $\tilde{\chi}_2^0$ production are expected. The second and third processes proceed via an off-shell squark, and the relative proportion of the first process to the other two depends on the precise relationship between M_3 and the squark masses. At the lowest values of M_3, the first process dominates entirely. The effect of the last two processes increases with rising gluino mass (with M_3 approaching the squark masses). For $M_3 > \approx 1$ TeV, the proportion of decays through the first process is at the level of a few percent, and one observes a relatively fixed proportion of the other two processes. The approximate branching ratios are relatively flat functions of M_3 for signal scenarios considered.

In gauge mediated SUSY scenarios a variety of mechanisms exist [32–36] to generate a Higgs boson mass as high as the observed value of $m_h = 125$ GeV, without changing the phenomenology of the models considered in this search. In the model used in this anlaysis, the lightest Higgs boson mass is specifically set to 125 GeV.

Previous searches for $\tilde{\tau}$ pair production, with the subsequent decay $\tilde{\tau} \to \tau\tilde{G}$ in the minimal GMSB model, have been reported by the LEP Collaborations ALEPH [37], DELPHI [38] and OPAL [39]. The analysis reported in this note extends the searches presented in Ref. [28] and comprises the full ATLAS dataset collected during the 2012 run, corresponding to an integrated luminosity of $(20.7 \pm 0.8)\,\text{fb}^{-1}$ [40] after applying beam, detector and data-quality requirements. The CMS Collaboration [41] recently presented the results of a supersymmetry search in events with τ leptons, jets and missing transverse momentum in 4.98 fb^{-1} of 7 TeV data in Ref. [42]. The results include interpretations in CMSSM and GMSB scenarios.

2 ATLAS detector

The ATLAS experiment is described in detail in Ref. [43]. It is a multi-purpose detector with a forward-backward symmetric cylindrical geometry and nearly 4π solid angle coverage. The inner tracking detector (ID) consists of a silicon pixel detector, a silicon strip detector and a transition radiation tracker. The ID is surrounded by a thin superconducting solenoid providing a 2 T magnetic field and by fine-granularity lead/liquid-argon (LAr) electromagnetic calorimeters. An iron/scintillating-tile calorimeter provides hadronic coverage in the central pseudorapidity[1] range. The endcap and forward regions are instrumented with liquid-argon calorimeters, with either steel, copper or tungsten as absorber material, for both electromagnetic and hadronic measurements. An extensive muon spectrometer system that incorporates large superconducting toroidal magnets surrounds the calorimeters.

3 Simulated samples

The Monte Carlo (MC) simulations used to evaluate the expected backgrounds and selection efficiencies for the SUSY models considered are similar to the ones used in Ref. [28]. The `ALPGEN` generator [44] is used to simulate samples of W and Z/γ^* events with up to five accompanying jets, where `CTEQ6L1` [45] is used for the parton density functions (PDFs). Z/γ^* events with $m_{ll} < 60$ GeV will be referred to in this note as "Drell-Yan". Top quark pair and di-boson (WW and WZ) pair production is simulated with `Sherpa` [46], while single top production is simulated with `MC@NLO` [47–49] and AcerMC [50] (for the t-channel), with the next-to-leading order (NLO) PDF set `CT10` [51]. The $t\bar{t}$ samples generated using the `ALPGEN` generator are also used to estimate systematic uncertainties. For the `MC@NLO` and `ALPGEN` samples, fragmentation and hadronisation are performed with `HERWIG` [52], using `JIMMY` [53] for the underlying event simulation. The decay of τ leptons and radiation of photons are simulated using `TAUOLA` [54, 55] and `PHOTOS` [56], respectively. The production of multijet events is simulated with `PYTHIA` 8 [57] using the `AUET2B` tune [58] and `MRST2007 LO*` [59] PDFs. For the comparison with data, all SM background cross sections are normalized to the results of higher-order calculations when available. The theoretical cross sections for W+jets and Z+jets are calculated with `DYNNLO` [60] with the `MSTW 2008NNLO` [61] PDF set. The inclusive $t\bar{t}$ cross section is calculated with `HATHOR 1.2` [62] using `MSTW 2008NNLO` PDFs. Single-top cross sections are taken from `MC@NLO`. For the diboson cross sections, `MCFM` [63] with the `MSTW 2008NLO` PDFs is used. For the minimal GMSB model considered in this analysis, the SUSY mass spectra are calculated using `SPHENO` v3.1.12 [64, 65]. For the nGM model, the SUSY mass and decay spectra are calculated using `SDECAY` 1.3b [66] and `HDECAY` 3.4 [67], run as part of the `SUSYHIT` package [68]. For the mSUGRA/CMSSM model the signal points have been produced with `SOFTSUSY` v3.6.1 [69]. The MC signal samples are produced using `HERWIG++` 2.5.1 [70] with `CTEQ6L1` PDFs. Signal cross sections are calculated to next-to-leading order in the strong coupling constant, adding the resummation of soft gluon emission at next-to-leading-logarithmic accuracy (NLO+NLL) [71–75]. The nominal cross section and the uncertainty are taken from an envelope of cross section predictions using different PDF sets and factorisation and renormalisation scales, as described in Ref. [76].

GMSB signal samples are generated on a parameter plane ranging from $\Lambda = 40$ TeV to $\Lambda = 120$ TeV and from $\tan\beta = 2$ to $\tan\beta = 60$. The mSUGRA/CMSSM signal samples are generated in the $m_0 - m_{1/2}$ plane, with a spacing of 200 to 500 GeV in m_0 and 50 GeV in $m_{1/2}$. The nGM samples are generated in the $m_{\tilde{\tau}} - m_{\tilde{g}}$ plane for fixed $\mu = 400$ GeV, with parameters ranging from $m_{\tilde{\tau}} = 117$ GeV to $m_{\tilde{\tau}} = 337$ GeV,

[1] ATLAS uses a right-handed coordinate system with its origin at the nominal interaction point (IP) in the centre of the detector and the z-axis along the beam pipe. The x-axis points from the IP to the centre of the LHC ring and the y-axis points upward. Cylindrical coordinates (R, ϕ) are used in the transverse plane, ϕ being the azimuthal angle around the beam pipe. The pseudorapidity is defined in terms of the polar angle θ as $\eta = -\ln\tan(\theta/2)$.

Table 2: Event selection criteria for the final states presented in this note.

	1τ SR	2τ GMSB SR	2τ nGM SR
Pre-selection	$p_{\mathrm{T}}^{\mathrm{jet1}} > 130$ GeV, $p_{\mathrm{T}}^{\mathrm{jet2}} > 30$ GeV $E_{\mathrm{T}}^{\mathrm{miss}} > 150$ GeV		
Taus	$N_{\tau}^{\mathrm{medium}} = 1$, $p_T^{\tau} > 30$ GeV	$N_{\tau}^{\mathrm{loose}} \geq 2$, $p_T^{\tau} > 20$ GeV	
Light leptons	$N_{\ell} = 0$		
QCD rejection	$\Delta(\phi_{jet_{1,2}-\mathbf{p}_{\mathrm{T}}{}^{\mathrm{miss}}}) > 0.3$ rad $E_{\mathrm{T}}^{\mathrm{miss}}/m_{\mathrm{eff}} > 0.3$	$\Delta(\phi_{jet_{1,2}-\mathbf{p}_{\mathrm{T}}{}^{\mathrm{miss}}}) > 0.3$ rad	
Signal cuts	$m_T^{\tau} > 140$ GeV $H_T > 800$ GeV	$m_{\mathrm{T}}^{\tau_1} + m_{\mathrm{T}}^{\tau_2} \geq 150$ GeV $H_T > 900$ GeV	$m_{\mathrm{T}}^{\tau_1} + m_{\mathrm{T}}^{\tau_2} \geq 250$ GeV $H_T > 600$ GeV $N_{\mathrm{jet}} \geq 4$

and from $m_{\tilde{g}} = 400$ GeV to $m_{\tilde{g}} = 1260$ GeV.

All samples are processed through the GEANT4-based simulation of the ATLAS detector [77,78]. The full simulation includes also a realistic treatment of the variation of the number of pp interactions per bunch crossing (pile-up) in the data, with an average of around 20 interactions per crossing.

4 Object reconstruction

The analyses presented use a hadronic trigger selecting events with at least one jet above 80 GeV and missing transverse momentum above 100 GeV. The offline selection thresholds were set in order to be in a region with uniform trigger efficiency for all data-taking periods, with the trigger efficiency exceeding 98% with respect to the offline selection for all final states considered.

Jets are reconstructed using the anti-k_t jet clustering algorithm [79] with distance parameter $R = 0.4$. Jet energies are calibrated to correct for upstream material, calorimeter non-compensation, pile-up, and other effects [80]. Jets are required to have transverse momenta (p_{T}) greater than 30 GeV and $|\eta| < 4.5$.

Muon candidates are identified by matching an extrapolated inner detector track and one or more track segments in the muon spectrometer [81, 82]. They are required to have $p_{\mathrm{T}} > 10$ GeV and $|\eta| < 2.4$. Electron candidates are required to satisfy $p_{\mathrm{T}} > 20$ GeV, $|\eta| < 2.47$ and to pass the "Medium++" identification criteria described in Ref. [83], re-optimized for 2012 conditions.

Tau leptons considered in this search are reconstructed through their hadronic decays. The τ reconstruction is seeded from jets with $p_{\mathrm{T}} > 10$ GeV. An η- and p_{T}-dependent energy calibration to the hadronic τ energy scale is applied. Discriminating variables based on tracking and observables sensitive to the transverse and longitudinal shape of the energy deposits of tau candidates in the calorimeter are used. These quantities are combined in a boosted decision tree (BDT) discriminator [84] to optimize their impact. Measurements of transition radiation and calorimeter information are used to veto electrons mis-identified as taus. Suitable τ lepton candidates must satisfy $p_{\mathrm{T}} > 20$ GeV, $|\eta| < 2.5$, and have one or three associated tracks of $p_{\mathrm{T}} > 1$ GeV with a charge sum of ± 1. A sample of $Z \to \tau\tau$ events is used to measure the efficiency of the BDT tau identification. The "loose" and "medium" working points in Ref. [84] are used herein and correspond to efficiencies of approximately 60% and 40% respectively, independent of p_{T}, with a rejection factor of $20 - 50$ against τ candidates built from hadronic jets ("fake" taus).

Following object reconstruction, overlaps between candidate jets, taus and light leptons are resolved. First, any tau candidate reconstructed within a distance $\Delta R = \sqrt{(\Delta\eta)^2 + (\Delta\phi)^2} = 0.2$ of an electron or muon is discarded. Jet candidates are then removed if they are reconstructed within a distance $\Delta R = 0.2$ of a tau or an electron. Next, muon candidates are rejected if they lie within $\Delta R = 0.2$ of a jet. Finally,

remaining electron and muon candidates are rejected if they are found within $0.2 < \Delta R < 0.4$ of a jet.

The missing transverse momentum vector $\mathbf{p}_{\mathrm{T}}{}^{\mathrm{miss}}$ (and its magnitude $E_{\mathrm{T}}^{\mathrm{miss}}$) is measured from the transverse momenta of identified jets, electrons, muons and all calorimeter clusters with $|\eta| < 4.5$ not associated to such objects [85]. For the purpose of the measurement of $E_{\mathrm{T}}^{\mathrm{miss}}$, τ leptons are not distinguished from jets.

After overlap removal, muon candidates are subject to an additional isolation requirement, i.e. the scalar sum of the transverse momenta of tracks within a cone $\Delta R < 0.2$ around the muon candidate, excluding the muon candidate track itself, must be less than 1.8 GeV for muons. Tracks selected for the muon isolation requirement have $p_{\mathrm{T}} > 1$ GeV and are associated to the primary vertex of the event. Isolated muons are used in the definition of a specific control region defined to cross check the Z+jets background estimation, as explained in Section 6.

Jets originating from decays of b-quarks are identified and used for separating the W and $t\bar{t}$ background contributions. They are identified by a neural network based algorithm, which combines the information from the track impact parameters with the search for decay vertices along the jet axis [86, 87]. A working point corresponding to 60% (< 0.5%) tagging efficiency for b-jets (light flavour or gluon jets) is chosen. This tagging efficiency has been obtained using simulated $t\bar{t}$ events.

5 Event Selection

Two mutually exclusive final states are considered for this search: events with only one hadronically decaying "medium" τ, no additional "loose" τ candidates and no muons or electrons, referred to in the following as "1τ "; events with two or more "loose" τ leptons and no muons or electrons, referred to as "2τ ".

The events have to fulfill a minimum set of requirements, in the following referred to as "preselection". Pre-selected events are required to have a reconstructed primary vertex [88] with at least five tracks (with $p_{\mathrm{T}} > 0.4$ GeV), at least one jet with $p_{\mathrm{T}} > 130$ GeV and large $E_{\mathrm{T}}^{\mathrm{miss}}$ ($E_{\mathrm{T}}^{\mathrm{miss}} > 150$ GeV). In addition, events are required to have at least a second jet with $p_{\mathrm{T}} > 30$ GeV.

Events are then passed through a further selection for each search channel. Remaining multijet events, where highly energetic jets are mis-measured, are rejected by requiring the azimuthal angle between the missing transverse momentum vector and either of the two leading jets to be greater than 0.3 rad. In addition, in the 1τ channel, the ratio $E_{\mathrm{T}}^{\mathrm{miss}}/m_{\mathrm{eff}}$ is required to be greater than 0.3, where the the effective mass m_{eff} is defined below. Three quantities characterising the kinematic properties of the event are used to further suppress the main background processes (W+jets, Z+jets and top, including $t\bar{t}$ and single-top events) in each final state:

- the transverse mass m_{T}^{τ} formed by $E_{\mathrm{T}}^{\mathrm{miss}}$and the p_{T} of the τ lepton in the 1τ and 2τ channels $m_{\mathrm{T}}^{\tau} = \sqrt{2p_{\mathrm{T}}^{\tau}E_{\mathrm{T}}^{\mathrm{miss}}(1 - \cos(\Delta\phi(\tau, E_{\mathrm{T}}^{\mathrm{miss}})))}$;
- the scalar sum H_{T} of the transverse momenta of τ lepton candidates and the two jets with the largest transverse momentum in the events: $H_{\mathrm{T}} = \sum p_{\mathrm{T}}^{\tau} + \sum_{i=1,2} p_{\mathrm{T}}^{\mathrm{jet_i}}$;
- the effective mass $m_{\mathrm{eff}} = H_{\mathrm{T}} + E_{\mathrm{T}}^{\mathrm{miss}}$.

For each of the final states, specific criteria are applied to the above quantities in order to define a signal region (SR), as summarized in Table 2. A requirement on m_{T}^{τ} is used to remove W+jets events in the 1τ analysis, while in the 2τ channel a requirement on $m_{\mathrm{T}}^{\tau_1} + m_{\mathrm{T}}^{\tau_2}$ is very effective in removing Z+jets events. A further requirement on H_{T} is applied in order to reduce the contribution of all remaining backgrounds. In the nGM signal region, a requirement on the number of jets in the event is also used, taking into

account that in the signal events high jet multiplicity is expected due to the three body decay of the gluino.

Figure 1 shows the m_{T}^{τ} distribution after all the requirements of the analysis except the ones on m_{T}^{τ} and H_{T}, as well as the H_{T} distribution after the requirement on m_{T}^{τ} for the 1τ channel in the GMSB signal region. Figure 2 shows the $m_{\mathrm{T}}^{\tau_1} + m_{\mathrm{T}}^{\tau_2}$ distribution after all the requirements of the analysis except the one on H_{T}, as well as the H_{T} distribution after the $m_{\mathrm{T}}^{\tau_1} + m_{\mathrm{T}}^{\tau_2}$ requirement for the 2τ channel in the GMSB signal region.

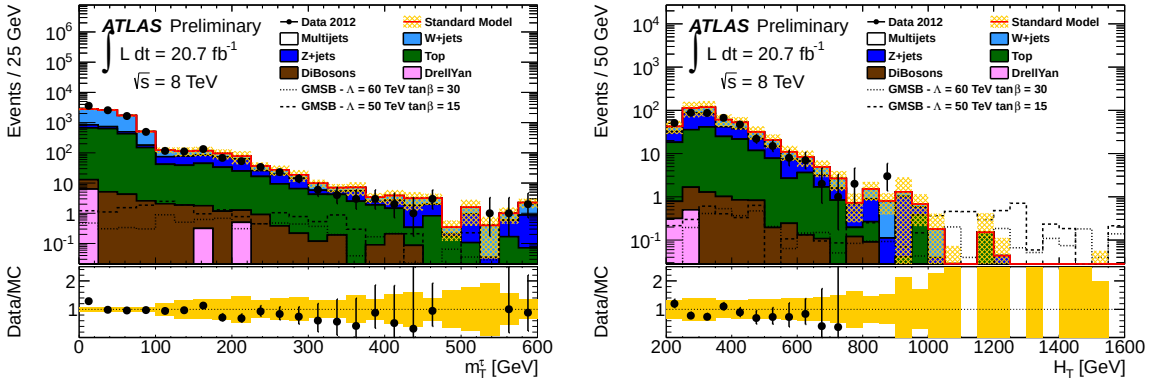

(a) (b)

Figure 1: Distribution of m_{T}^{τ} after all analysis requirements but the the requirement on m_{T}^{τ} and the final requirement on H_{T} (a) and of H_{T} after the m_{T}^{τ} requirement (b) for the 1τ signal region. Data are represented by the points. The SM prediction includes the data driven corrections discussed in the text. The shaded band centered around the total SM background indicates the statistical and systematic uncertainty on the background expectation. Monte Carlo events are normalized to data in the control region corresponding to m_{T}^{τ} below 130 GeV, resulting in a narrowing of the systematic uncertainty for low m_{T}^{τ} values. Also shown is the expected signal from typical GMSB samples. No events in data surviving all the analysis requirements end up in the overflow bin of the data distribution.

Figure 3 shows the H_{T} distribution after all the requirements of the analysis except the final requirements on H_{T} and the number of jets, as well as the N_{Jet} distribution after the H_{T} requirement for the 2τ channel in the nGM signal region.

6 Background estimation

For each final state, the SM background expectations predicted by MC simulation in the signal regions (SRs) are corrected, after all selection criteria are applied, by means of control regions (CRs) which are chosen such that a specific background process is enriched while any overlap with each SR is avoided. This is done to reduce possible mis-modelling of τ mis-identification probabilities and kinematics in the MC simulations. MC studies show that the τ mis-identification probability is, to a good approximation, independent of the kinematic variables used to separate the SR from the CRs, so that the measured ratio of the data to MC event yields in the CR can be used to compute scaling factors (SFs) to correct the MC background prediction in the SR. Correlations between different samples in the various CRs are taken into account by considering the matrix equation $\vec{N}^{\mathrm{data}} = A\,\vec{\omega}$ where $\vec{N}^{\mathrm{data}}$ is the observed number of data events in each CR, after subtracting the expected number of multijet events and any

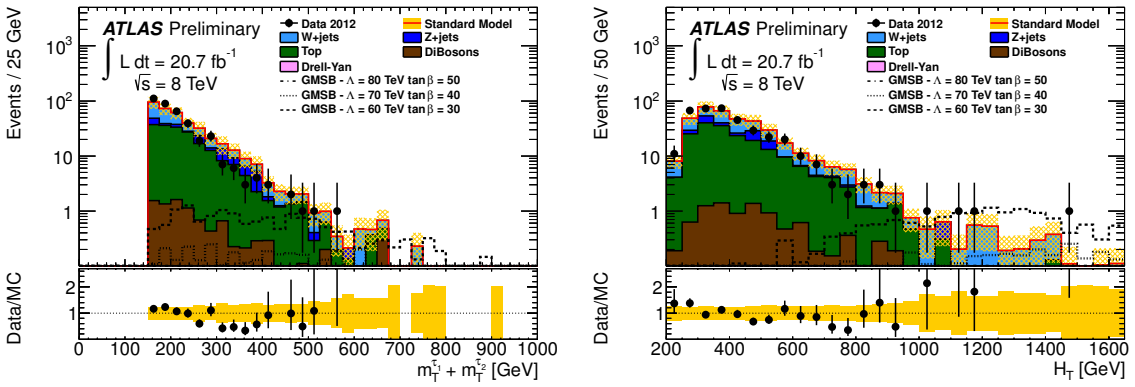

(a) (b)

Figure 2: Distribution of $m_{\mathrm{T}}^{\tau_1} + m_{\mathrm{T}}^{\tau_2}$ after all analysis requirements but the final requirement on H_{T} (a) and of H_{T} after the $m_{\mathrm{T}}^{\tau_1} + m_{\mathrm{T}}^{\tau_2}$ requirement (b) for the 2τ final state in the GMSB signal region. Data are represented by the points. The SM prediction includes the data driven corrections discussed in the text. The shaded band centered around the total SM background indicates the statistical and systematic uncertainty on the background expectation. Also shown is the expected signal from typical GMSB samples. No events in data surviving all the analysis requirements end up in the overflow bin of the data distribution.

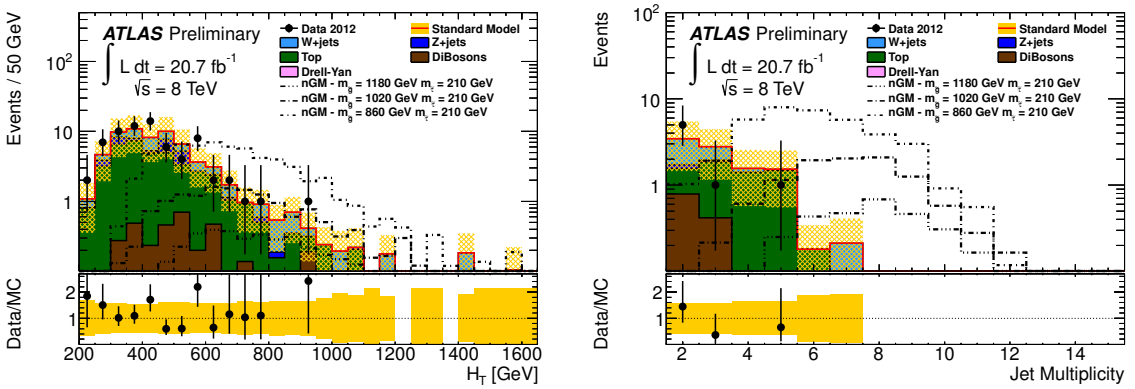

(a) (b)

Figure 3: Distribution of H_{T} in the nGM signal region after all analysis requirements but the final ones on H_{T} and the number of jets (a) and of N_{Jet} after the H_{T} requirement (b) for the 2τ final state. Data are represented by the points. The SM prediction includes the data driven corrections discussed in the text. The shaded band centered around the total SM background indicates the statistical and systematic uncertainty on the background expectation. Also shown is the expected signal from typical nGM samples. No events in data surviving all the analysis requirements end up in the overflow bin of the data distribution.

remaining sub-dominant background contribution obtained from MC. The matrix A is obtained from the MC expectation for the number of events originating from each of the backgrounds (top, W and Z). The vector $\vec{\omega}$ of scaling factors is then computed by inverting the matrix A.

The dominant backgrounds to the 1τ SR arise from Z and W boson production in association with jets, and from top production. Events can be divided into those in which a true tau exists and those in which a jet is mis-identified as a tau. Since the composition of true and fake (mis-identified) taus in the control region and signal region may differ, it is necessary to measure separate scaling factors for the two cases. To this end, a two-dimensional control region is defined, where in one dimension m_{T}^{τ} is used to separate true and fake taus, and in the other the b-tagging is used to provide a top enriched or depleted sample. Due to the complex nature of the τ lepton decays, the Jacobian peak in the m_{T}^{τ} distribution is very broad and therefore not clearly visible. The true/fake composition in the background samples as well as its relationship to m_{T}^{τ} has been extensively studied using MC events. The full list of selection requirements for these control regions, after the pre-selection, tau and light lepton veto requirements are applied, is provided in Table 3. The matrix A is a 4×4 matrix from which the SFs for W events with a true τ candidate, W/Z events with a fake τ candidate, and top events with either a true or a fake τ candidate are obtained. In Z+jets events, the background is completely dominated by Z decays to neutrinos, and therefore the τ candidate is always a mis-identified jet. For this reason, the scaling factor is obtained from the same fake CR defined for W+jets events. Typical scaling factors obtained for the various MC samples in the fake CR are ~ 0.7 for W+jets and Z+jets and $\sim$0.6 for $t\bar{t}$. In the true CR, these factors are ~ 0.9 for W+jets and ~ 1.0 for $t\bar{t}$. To obtain the uncertainties on the scaling factors, all contributing parameters are varied according to their uncertainties, the procedure is repeated and new scaling factors are obtained. The width of the distribution of the resulting scaling factors is then used as their uncertainty. Typical uncertainties are of order 20–70%, depending on the control region. As a cross check to validate the estimate of the scaling factors for the Z+jets background, the data/MC ratio from $\mathrm{Z} \to \ell^{+}\ell^{-}$ decays is measured in the Z+jets CR defined in Table 3. The scaling factors obtained for the Z+jets events with the two methods are in good agreement.

The contribution arising from multijet background processes due to fake taus is estimated using a data-driven "ABCD" method. The four regions are indicated in Table 4. Region D is similar to the SR, except for the fact that the requirement on $E_{\mathrm{T}}^{\mathrm{miss}}/m_{\mathrm{eff}}$ is reverted and there is no requirement on H_{T}. In order to estimate the total yield from multijet events in the SR, the number of events obtained in region D, calculated by multipling the number of events in data in region C by the ratio of events in data in region A and B, is then multiplied by the fraction of events passing the final cuts on H_{T} and $E_{\mathrm{T}}^{\mathrm{miss}}/m_{\mathrm{eff}}$. This fraction is derived in region A, after checking that it has little dependence on the requirements used to define the different multijet regions. In each region, the non-multijet contribution is estimated using MC simulation and is subtracted from the data. Extra-loose taus are defined by taking the nominal (medium) tau selection and relaxing the BDT discriminant, charge and number of associated tracks criteria.

In the 2τ analysis, the W and top backgrounds are dominated by events in which one τ candidate is a true τ and the others are mis-reconstructed from hadronic activity in the final state. The additional contribution from Z+jets events is dominated by final states with $Z \to \tau\tau$ decays. The CRs defined for the estimation of these backgrounds have a negligible contamination from multijet events thanks to the requirement on $\Delta(\phi_{jet_{1,2}-\mathbf{p}_{\mathrm{T}}{}^{\mathrm{miss}}})$ and the requirement of two or more τ lepton candidates. The definitions of the 2τ control regions are given in Table 3. In the GMSB analysis, three CRs are defined (for W+jets, Z+jets and $t\bar{t}$ events). Given that the true and fake τ candidates composition in the CR and SR is the same (as checked in truth level MC studies), there is no need to separate the CRs between true dominated and fake dominated. The matrix A in this case is a 3×3 matrix from which the SFs for W, Z and top events are obtained. Typical scaling factors obtained for the various MC samples are ~ 0.8 for the W+jets, ~ 1.1 for the Z+jets and ~ 0.6 for $t\bar{t}$. The uncertainties on the SFs are obtained in the same way as for the 1τ channel. Typical uncertainties are of order 40 %.

In the nGM signal region top events are the overall dominant background and therefore only one CR is defined. In this case, the CR to estimate the scale factor is defined to mimic at best the SR selection, with tight requirement on $m_{\mathrm{T}}^{\tau_1} + m_{\mathrm{T}}^{\tau_2}$ and on the jet multiplicity. The scale factor obtained in this case is

Table 3: Definition of the background control regions (CRs) used to estimate the yield of background candidates in the 1τ and 2τ final states.

Background	1τ	2τ GMSB	2τ nGM
top	$\Delta(\phi_{jet_{1,2}-\mathbf{p}_{\mathrm{T}}^{\mathrm{miss}}}) > 0.3$ rad $m_{\mathrm{T}}^{\tau} < 80$ GeV (true τ) *or* 80 GeV $< m_{\mathrm{T}}^{\tau} < 130$ GeV (fake τ) $E_{\mathrm{T}}^{\mathrm{miss}}/\mathrm{m_{eff}} > 0.3$ $N_{\mathrm{b-tag}} \geq 1$	$\Delta(\phi_{jet_{1,2}-\mathbf{p}_{\mathrm{T}}^{\mathrm{miss}}}) > 0.3$ rad $m_{\mathrm{T}}^{\tau_1} + m_{\mathrm{T}}^{\tau_2} \geq 150$ GeV $H_{\mathrm{T}} < 550$ GeV $N_{\mathrm{b-tag}} \geq 1$	$\Delta(\phi_{jet_{1,2}-\mathbf{p}_{\mathrm{T}}^{\mathrm{miss}}}) > 0.3$ rad $m_{\mathrm{T}}^{\tau_1} + m_{\mathrm{T}}^{\tau_2} \geq 250$ GeV $N_{\mathrm{Jet}} \geq 4$ $H_{\mathrm{T}} < 550$ GeV $N_{\mathrm{b-tag}} \geq 1$
W+jets		$\Delta(\phi_{jet_{1,2}-\mathbf{p}_{\mathrm{T}}^{\mathrm{miss}}}) > 0.3$ rad $m_{\mathrm{T}}^{\tau_1} + m_{\mathrm{T}}^{\tau_2} \geq 150$ GeV $H_{\mathrm{T}} < 550$ GeV $N_{\mathrm{b-tag}} = 0$	
W+jets (true)	$\Delta(\phi_{jet_{1,2}-\mathbf{p}_{\mathrm{T}}^{\mathrm{miss}}}) > 0.3$ rad $m_{\mathrm{T}}^{\tau} < 80$ GeV $E_{\mathrm{T}}^{\mathrm{miss}}/\mathrm{m_{eff}} > 0.3$ $\Delta\phi(\tau, E_{\mathrm{T}}^{\mathrm{miss}}) > 0.2$ $N_{\mathrm{b-tag}} = 0$		
W/Z+jets (fake)	$\Delta(\phi_{jet_{1,2}-\mathbf{p}_{\mathrm{T}}^{\mathrm{miss}}}) > 0.3$ rad 80 GeV $< m_{\mathrm{T}}^{\tau} < 130$ GeV $E_{\mathrm{T}}^{\mathrm{miss}}/\mathrm{m_{eff}} > 0.3$ $N_{\mathrm{b-tag}} = 0$		
Z+jets	2 opposite sign μ ($p_{\mathrm{T}} > 15$ GeV, $\lvert\eta\rvert < 2.4$) $\geq$2 jets (130 GeV, 30 GeV) a tau with $p_T > 20$ GeV 82 GeV$< m_{\mu^+\mu^-} <$ 100 GeV	$\Delta(\phi_{jet_{1,2}-\mathbf{p}_{\mathrm{T}}^{\mathrm{miss}}}) > 0.3$ rad $m_{\mathrm{T}}^{\tau_1} + m_{\mathrm{T}}^{\tau_2} < 80$ GeV $H_{\mathrm{T}} < 550$ GeV	
Multi-jet	ABCD method	$\Delta(\phi_{jet_{1,2}-\mathbf{p}_{\mathrm{T}}^{\mathrm{miss}}}) < 0.3$ rad $E_{\mathrm{T}}^{\mathrm{miss}}/m_{\mathrm{eff}} < 0.4$	

Table 4: Definitions of QCD regions used in ABCD method for the 1τ analysis. The requitement on H_{T} is not applied in the definition of these control regions.

	Extra Loose τ	Nominal τ
$\Delta\left(\phi_{jet_{1,2}-\mathbf{p}_{\mathrm{T}}{}^{\mathrm{miss}}}\right) < 0.3$ no cut on $E_{\mathrm{T}}^{\mathrm{miss}}/m_{\mathrm{eff}}$	Control region A	Control region B
$\Delta\left(\phi_{jet_{1,2}-\mathbf{p}_{\mathrm{T}}{}^{\mathrm{miss}}}\right) > 0.3$ $E_{\mathrm{T}}^{\mathrm{miss}}/m_{\mathrm{eff}} < 0.3$	Control region C	Region D

of the order of 0.4 , with an uncertainty of 30 %.

The multijet background expectation for the 2τ final states is computed by using MC to model the shape of the background, but with a normalisation taken from a multijet dominated CR defined by inverting the $\Delta(\phi_{jet_{1,2}-\mathbf{p}_{\mathrm{T}}{}^{\mathrm{miss}}})$ requirement and not applying the $m_{\mathrm{T}}^{\tau_1} + m_{\mathrm{T}}^{\tau_2}$ and H_{T} selection. In addition, the ratio $E_{\mathrm{T}}^{\mathrm{miss}}/m_{\mathrm{eff}}$ is required to be smaller than 0.4 to increase the purity of this CR. To increase the size of the event sample, an extra loose tau selection is defined by relaxing the tau BDT selection criterion. The MC events passing this selection are then reweighted by applying, to each tau in an event, a measured probability that an extra loose tau will pass the loose tau identification. This gives a sample of MC events with loose taus that can be passed through the rest of the analysis in order to obtain the multijet yield in the signal region.

In both the 1τ and 2τ channels, the sub-dominant di-boson and Drell-Yan background contributions are estimated using MC simulations. In both analyses the contribution from Drell-Yan is found to be negligible.

7 Systematic uncertainties on the background

Various systematic uncertainties have been studied and the effect on the number of expected background events in each one of the channels presented here has been taken into account, following the approach of Ref. [28]. The dominant systematic uncertainties in the different channels are summarised in Table 5, with the exception of the luminosity uncertainty which is discussed below.

The theoretical uncertainty on the MC-based extrapolation of the W+jets and $t\bar{t}$ backgrounds from the CR into the SR is estimated using alternative MC samples. These MC samples have been obtained by varying the renormalisation and factorisation scales, the functional form of the factorisation scale and the matching threshold in the parton shower process in the generators used for the simulation of the events described in Section 3. Moreover, in case of $t\bar{t}$ processes, the difference in the background estimation obtained using the `SHERPA` and `ALPGEN` MC generators is taken as the uncertainty on the MC generator.

Systematic uncertainties on the jet energy scale (JES) and jet energy resolution (JER) [80] are applied in MC to the jet candidates and propagated through the analysis. The difference in the number of expected background events obtained with the nominal MC simulation after applying the JES and JER uncertainty variations is taken as the systematic uncertainty.

The effect of the τ energy scale (TES) uncertainty on the expected background is estimated in a similar way. The uncertainties from the jet and τ energy scale are treated as fully correlated.

The uncertainties on the background estimation due to the τ identification efficiency depend on the τ identification algorithm ("loose" or "medium"), the kinematics of the τ sample and the number of associated tracks. In both 1τ and 2τ channel they are less than 0.5%.

To account for mis-modelling of pile-up in the MC, a re-weighting procedure of all MC samples according to the measured number of mean interactions per bunch crossing in data is done. A systematic uncertainty associated with this procedure is taken into account by changing the nominal value for the

Table 5: Overview of the major systematic uncertainties on the total expected background in each signal region for the background estimates in the channels presented in this note.

Source of Uncertainty	1τ	2τ GMSB	2τ nGM
CR to SR Extrapolation	15%	18%	50%
Jet Energy Resolution	4.5%	7.1%	11%
Jet Energy Scale	16%	5.1%	4.9%
Tau Energy Scale	18%	1.5%	7.5%
Pileup re-weighting	5.3%	7.0%	7.7%

average interactions per bunch crossing in data by 10%, repeating the analysis and determining the relative deviations from the nominal yields.

The preliminary uncertainty on the luminosity of the 2012 data is 3.6% based on the calibration procedure described in Ref. [40]. The effect of this uncertainty on the normalization of the Z+jets, Drell-Yan and di-boson samples, for which scale factors derived from control regions were not applied, is also considered.

The limited size of the MC samples used for background estimation gives rise to statistical uncertainties which are also taken into account.

The total systematic uncertainties obtained in the 1τ, 2τ GMSB and 2τ nGM regions are 29%, 23% and 54% respectively.

8 Signal efficiencies and systematic uncertainties

The GMSB and nGM signal samples have been described in Section 3. The cross section for strong production, for which this analysis has the largest sensitivity, decreases faster than the cross section for slepton- and gaugino production, such that for large values of Λ the selection efficiency with respect to the total SUSY production decreases.

In the GMSB signal scenarios, in the high $\tan\beta$ region the acceptance times efficiency is of the order of 1% for the 1τ channel. For low $\tan\beta$ values, it drops to 0.1%. For large Λ it rises to values of 10%. For the 2τ channel in the high $\tan\beta$ region the acceptance times efficiency is of the order of 6% and drops to 1% for low $\tan\beta$ values.

The total systematic uncertainty on the signal selection from the various sources discussed in Section 7 is between 1–10% for the 1τ channel for most of the signal samples studied. For low $\tan\beta$ and high Λ it rises up to 60%. For the 2τ channel it amounts to 10–15% for most of the parameter space with an increase to up to 35% for the highest Λ region studied and low $\tan\beta$.

In the nGM scenarios, the sensitivity to chargino/neutralino production is negligible because of the stringent $E_{\mathrm{T}}^{\mathrm{miss}}$and jet p_{T} requirements. It is therefore the gluino pair production that is the dominant process. The gluino pair production cross section is primarily a function of $m_{\tilde{g}}$, dropping from 17.2 pb for $m_{\tilde{g}} = 400$ GeV to 7 fb for $m_{\tilde{g}} = 1100$ GeV. The acceptance for the 2τ analysis is of the order of 15% for high $m_{\tilde{g}}$, independent of $m_{\tilde{\tau}}$, and it drops to ~2% for low $m_{\tilde{g}}$. The efficiency ranges from around 30% to 80–90%, with the higher values being observed in the low $m_{\tilde{g}}$ region. The 1τ analysis has negligible sensitivity to the scenarios, so no interpretation of the 1τ result in nGM is presented. The total experimental systematic uncertainty on the signal selection from the various sources discussed in Section 7 is between 10–30%.

In the mSUGRA signal plane the acceptance times efficiency ranges from below the percent level to around 7% for the 1τ channel, with the higher values being observed in the low $m_{1/2}$ region. The 2τ

channel has vanishing acceptance due to the lack of a second high-p_{T} τ, which is why the 2τ analysis is not interpreted in this context. The total systematic uncertainty on the signal selection from the various sources discussed in Section 7 is between 2% to 20% across the plane. It rises up to 50% at the lowest $m_{1/2}$ region studied and up to 80% for individual signal points at the highest $m_{1/2}$ values.

The nominal cross sections and uncertainties in the different models discussed in this note are taken from an envelope of cross section predictions using different PDF sets and factorisation and renormalisation scales, as described in Ref. [76]. This procedure is the same as detailed in Ref. [28] The uncertainties are calculated for individual SUSY production processes and for each model point in the GMSB, mSUGRA and nGM plane. The overall theoretical cross section uncertainties are between 15–30% in GMSB, 10–30% in mSUGRA and 15–40% in nGM.

9 Results

Table 6 summarizes the number of observed events in the two channels in data and the number of expected background events. No significant excess is observed in any of the signal regions. From the number of data events observed and the expected number of background events, an upper limit at 95% Confidence Level (CL) on the observed event yield from any scenario of physics beyond the SM is calculated in the 1τ and 2τ channel, respectively. These upper limits translate into a 95% CL observed (expected) upper limit on the visible cross section for new phenomena for each of the final states, defined by the product of cross section, branching fraction, acceptance and efficiency for the selections defined in Section 5. The results are summarized in Table 6 for all channels. The limits are computed using the profile likelihood ratio method [89] and the CL_s criterion [90]. Uncertainties on the background and signal expectations are treated as Gaussian-distributed nuisance parameters in the likelihood fit.

In order to produce the strongest possible 95% CL limit on the GMSB model parameters Λ and $\tan\beta$, a statistical combination of the 1τ and 2τ channels is performed, in which the full likelihood function that represents the outcome of the combination is used. The combination profits from the fact that the two final states are statistically independent. The limit is calculated including all experimental uncertainties on the background and signal expectations and theoretical uncertainties on the background. The resulting observed and expected limits for the combination of final states are shown in Fig. 4. The yellow band around the expected exclusion limit represents the 1σ statistical and systematic uncertainty on the expected background. The influence of the theoretical uncertainties on the signal cross section on the limit is indicated by the dashed red lines around the observed limit. From this, a limit on the SUSY breaking scale Λ of 54 TeV is determined, independent of $\tan\beta$. The limit on Λ increases to 70 TeV for high $\tan\beta$ ($\tan\beta > 50$).

Figure 5 shows the expected and observed exclusion limit obtained when interpreting the 1τ analysis result using the mSUGRA/CMSSM model plane. Values of m_0 up to 860 GeV for low $m_{1/2}$, and values of $m_{1/2}$ up to 650 GeV for low m_0 are excluded by this analysis.

Figure 6 shows the expected and observed exclusion limit in the nGM scenarios using the dedicated high jet multiplicity signal region of the 2τ analysis. Signal contaminations in the dedicated top CR are of the order of 10% for gluino mass of the order of 1 TeV and are taken into account in the limit computation. Exclusion limits on the mass of the gluino are set to 1140 GeV, independent of the $\tilde{\tau}$ mass.

10 Conclusions

A search for SUSY in final states with jets, $E_{\mathrm{T}}^{\mathrm{miss}}$ and one or more hadronically decaying τ leptons is performed using 20.7 fb^{-1} of $\sqrt{s} = 8$ TeV pp collision data recorded with the ATLAS detector at the LHC. No excess above the expected SM backgrounds is observed. The results are used to set model-

Table 6: Number of expected background events and data yields in the 1τ and 2τ final states. Where possible, the uncertainties are separated in statistical (first) and systematic (second). The SM prediction is computed taking into account correlations between the different uncertainties. Also shown are the number of expected signal MC events for one GMSB point (Λ=50 TeV, tanβ=30), an nGM signal point with $m_{\tilde{\tau}} = 210$ GeV and $m_{\tilde{g}} = 1020$ GeV and an mSUGRA point with $m_0 = 400$ GeV and $m_{1/2} = 650$ GeV.
The resulting 95% Confidence Level (CL) limit on the number of observed (expected) signal events and on the visible cross sections from any new physics scenario for each of the final states is shown, taking into account the observed events in data and the background expectations.

–	1τ	2τ GMSB region	2τ nGM region
Multi-jet	0.03 ± 0.01	0.14 ± 0.04	0.04 ± 0.02
W + jets	$1.9 \pm 0.5 \pm 0.7$	$3.8 \pm 1.1 \pm 0.9$	$0.3 \pm 0.2 \pm 0.4$
Z + jets	$2.1 \pm 1.2 \pm 1.7$	$0.3 \pm 0.3 \pm 0.5$	$0.02 \pm 0.02 \pm 0.01$
top	$0.7 \pm 0.6 \pm 0.3$	$2.4 \pm 0.7 \pm 1.4$	$3.1 \pm 1.0 \pm 1.7$
di-boson	$0.1 \pm 0.1 \pm 0.1$	$0.6 \pm 0.2 \pm 0.2$	$0.02 \pm 0.02 \pm 0.02$
Total background	$4.9 \pm 1.5 \pm 1.3$	$7.2 \pm 1.3 \pm 1.6$	$3.5 \pm 1.1 \pm 1.9$
Data	3	5	1
Signal MC Events			
GMSB5030	9 ± 2	36 ± 2	–
nGM 210-1020	–	–	10 ± 1
mSUGRA 400-650	6 ± 1	–	–
Obs (exp) limit on signal events	8.2 ($8.3^{+3.1}_{-2.2}$)	8.4 ($9.9^{+4.8}_{-3.3}$)	5.4 ($7.6^{+3.1}_{-2.2}$)
Obs limit on Cross Section (fb)	0.40	0.41	0.26

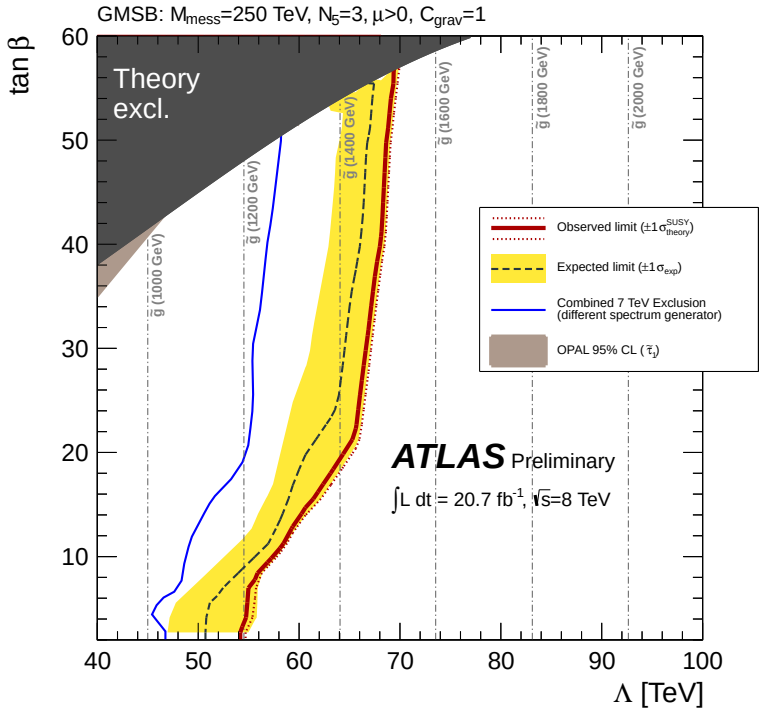

Figure 4: Expected and observed 95% CL lower limits on the minimal GMSB model parameters Λ and $\tan\beta$ using a combination of the 1τ and 2τ analysis. The result is obtained using 20.7 fb^{-1} of $\sqrt{s} = 8$ TeV ATLAS data. The dark grey area indicates the region which is theoretically excluded due to unphysical sparticle mass values. Additional model parameters are $M_{\text{mess}} = 250$ TeV, $N_5 = 3$, $\mu > 0$ and $C_{\text{grav}} = 1$. The OPAL limits on the $\tilde{\tau}$ mass [39] and the previous ATLAS [28] limits are shown. For the latter, a different mass spectrum generator had been employed.

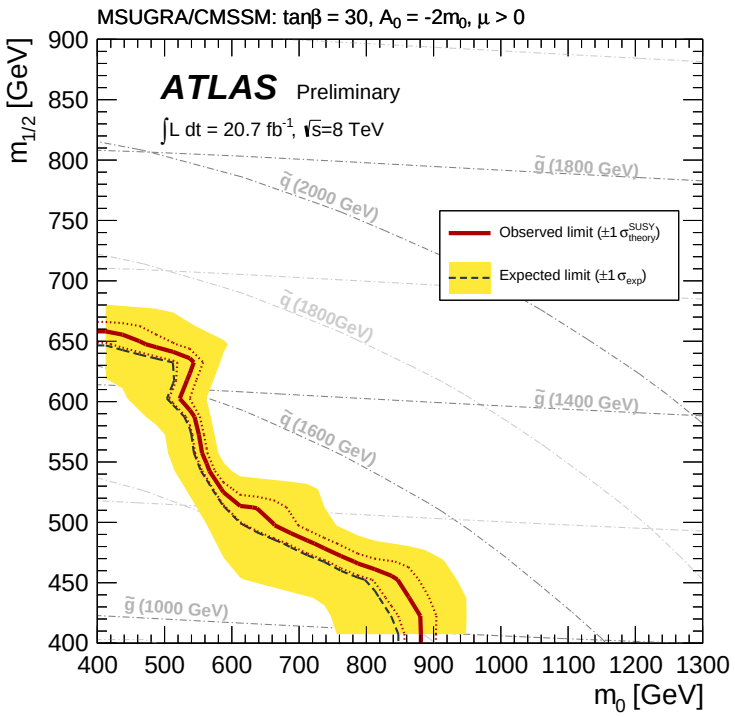

Figure 5: Expected and observed 95% CL lower limits on the mSUGRA/CMSSM model parameters m_0 and $m_{1/2}$ for the 1τ analysis. Additional model parameters are $A_0 = -2\times m_0$, $\tan\beta = 30$ and $sign(\mu) = +1$.

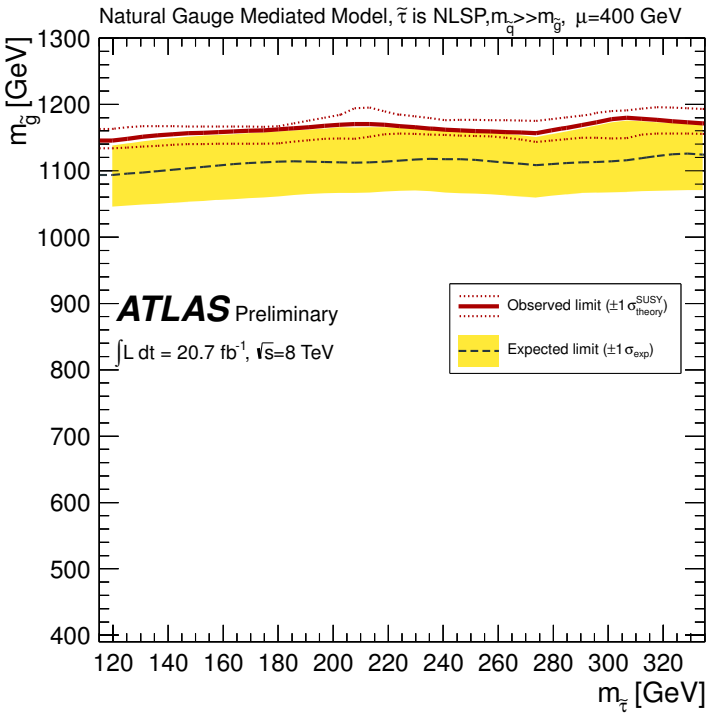

Figure 6: Expected and observed 95% CL lower limits on the simplified nGM model parameters $m_{\tilde{\tau}}$ and $m_{\tilde{g}}$ for the 2τ analysis. Additional squark and slepton mass parameters are set to 2.5 TeV, $M_1 = M_2 =$ 2.5 TeV, and all trilinear coupling terms are set to zero. Also, the parameter μ is fixed to $\mu = 400$ GeV.

independent 95% CL upper limits on the number of signal events from new phenomena and corresponding upper limits on the visible cross section. Limits on model parameters are set for a minimal GMSB and natural Gauge Mediation models. A limit on the SUSY breaking scale Λ of 54 TeV is determined, independent of $\tan\beta$, for the minimal GMSB model. The limit on Λ increases to 70 TeV for high $\tan\beta$ ($\tan\beta > 50$). Additionally, the 1τ result is interpreted using a mSUGRA/CMSSM model, and limits in the $m_0 - m_{1/2}$ plane are obtained. In a natural Gauge Mediation model the result of the 2τ analysis in an optimised signal region can be translated into a limit on the gluino mass of 1140 GeV, independent of the $\tilde{\tau}$ mass, provided the $\tilde{\tau}$ is the NLSP.

References

[1] H. Miyazawa, *Baryon Number Changing Currents*, Prog. Theor. Phys. **36 (6)** (1966) 1266–1276.

[2] P. Ramond, *Dual Theory for Free Fermions*, Phys. Rev. **D3** (1971) 2415–2418.

[3] Y. A. Golfand and E. P. Likhtman, *Extension of the Algebra of Poincare Group Generators and Violation of p Invariance*, JETP Lett. **13** (1971) 323.

[4] A. Neveu and J. H. Schwarz, *Factorizable dual model of pions*, Nucl. Phys. **B31** (1971) 86.

[5] A. Neveu and J. H. Schwarz, *Quark Model of Dual Pions*, Phys. Rev. **D4** (1971) 1109.

[6] J. Gervais and B. Sakita, *Field theory interpretation of supergauges in dual models*, Nucl. Phys. **B34** (1971) 632–639.

[7] D. V. Volkov and V. P. Akulov, *Is the Neutrino a Goldstone Particle?*, Phys. Lett. **B46** (1973) 109.

[8] J. Wess and B. Zumino, *A Lagrangian Model Invariant Under Supergauge Transformations*, Phys. Lett. **B49** (1974) 52.

[9] J. Wess and B. Zumino, *Supergauge Transformations in Four-Dimensions*, Nucl. Phys. **B70** (1974) 39.

[10] M. Dine and W. Fischler, *A Phenomenological Model of Particle Physics Based on Supersymmetry*, Phys. Lett. **B110** (1982) 227.

[11] L. Alvarez-Gaume, M. Claudson, and M. Wise, *Low-energy Supersymmetry*, Nucl. Phys. **B207** (1982) 96.

[12] C. R. Nappi and B. A. Ovrut, *Supersymmetric Extension of the SU(3) x SU(2) x U(1) Model*, Phys. Lett. **B113** (1982) 175.

[13] M. Dine and A. E. Nelson, *Dynamical supersymmetry breaking at low-energies*, Phys. Rev. **D48** (1993) 1277.

[14] M. Dine, A. E. Nelson, and Y. Shirman, *Low-energy dynamical supersymmetry breaking simplified*, Phys. Rev. **D51** (1995) 1362.

[15] M. Dine, A. E. Nelson, Y. Nir, and Y. Shirman, *New Tools for Low-energy Dynamical Supersymmetry Breaking*, Phys. Rev. **D53** (1996) 2658.

[16] A. H. Chamseddine, R. Arnowitt, and P. Nath, *Locally Supersymmetric Grand Unification*, Phys. Rev. Lett. **49** (1982) 970.

[17] R. Barbieri, S. Ferrara, and C. A. Savoy, *Gauge Models with Spontaneously Broken Local Supersymmetry*, Phys. Lett. **B119** (1982) 343.

[18] L. E. Ibanez, *Locally Supersymmetric SU(5) Grand Unification*, Phys. Lett. **B118** (1982) 73.

[19] L. J. Hall, J. D. Lykken, and S. Weinberg, *Supergravity as the Messenger of Supersymmetry Breaking*, Phys. Rev. **D27** (1983) 2359–2378.

[20] N. Ohta, *Grand Unified Theories Based on Local Supersymmetry*, Prog. Theor. Phys. **70** (1983) 542.

[21] G. L. Kane, C. F. Kolda, L. Roszkowski, and J. D. Wells, *Study of constrained minimal supersymmetry*, Phys. Rev. **D49** (1994) 6173–6210.

[22] J. Barnard, B. Farmer, T. Gherghetta, and M. White, *Natural gauge mediation with a bino NLSP at the LHC*, Phys.Rev.Lett. **109** (2012) 241801.

[23] P. Fayet, *Supersymmetry and Weak, Electromagnetic and Strong Interactions*, Phys. Lett. **B64** (1976) 159.

[24] P. Fayet, *Spontaneously Broken Supersymmetric Theories of Weak, Electromagnetic and Strong Interactions*, Phys. Lett. **B69** (1977) 489.

[25] G. R. Farrar and P. Fayet, *Phenomenology of the Production, Decay, and Detection of New Hadronic States Associated with Supersymmetry*, Phys. Lett. **B76** (1978) 575.

[26] P. Fayet, *Relations Between the Masses of the Superpartners of Leptons and Quarks, the Goldstino Couplings and the Neutral Currents*, Phys. Lett. **B84** (1979) 416.

[27] S. Dimopoulos and H. Georgi, *Softly Broken Supersymmetry and SU(5)*, Nucl. Phys. **B193** (1981) 150.

[28] ATLAS Collaboration, *Search for Supersymmetry in events with large missing transverse momentum, jets and at least one tau lepton in 7 TeV proton-proton collision data with the ATLAS detector*, Eur. Phys. J. **C 72** (2012) 2215.

[29] ATLAS Collaboration, *Observation of a new particle in the search for the Standard Model Higgs boson with the ATLAS detector at the LHC*, Phys.Lett. **B716** (2012) 1–29.

[30] CMS Collaboration, CMS Collaboration, *Observation of a new boson at a mass of 125 GeV with the CMS experiment at the LHC*, Phys.Lett. **B716** (2012) 30–61.

[31] M. Buican, P. Meade, N. Seiberg, and D. Shih, *Exploring General Gauge Mediation*, JHEP **0903** (2009) 016, arXiv:0812.3668 [hep-ph].

[32] N. Craig, D. Green, and A. Katz, *(De)Constructing a natural and flavorful supersymmetric Standard Model*, JHEP **1107** (2011) 045.

[33] R. Auzzi, A. Giveon, and S. B. Gudnason, *Flavor of quiver-like realizations of effective supersymmetry*, JHEP **1202** (2012) 069.

[34] C. Csaki, L. Randall, and J. Terning, *Light stops from Seiberg duality*, arXiv:1201.1293 [hep-ph].

[35] G. Larsen, Y. Nomura, and H. L. Roberts, *Supersymmetry with light stops*, JHEP **1206** (2012) 032.

[36] N. Craig, S. Dimopoulos, and T. Gherghetta, *Split families unified*, JHEP **1204** (2012) 116.

[37] ALEPH Collaboration, A. Heister et al., *Search for Gauge Mediated SUSY Breaking Topologies in e^+e^- Collisions at Center-of-mass Energies up to 209 GeV*, Eur. Phys. J. **C25** (2002) 339.

[38] DELPHI Collaboration, J. Abdallah et al., *Search for supersymmetric particles in light gravitino scenarios and sleptons NLSP*, Eur. Phys. J. **C27** (2003) 153.

[39] OPAL Collaboration, G. Abbiendi et al., *Searches for gauge-mediated supersymmetry breaking topologies in e+ e- collisions at LEP2*, Eur. Phys. J. **C46** (2006) 307.

[40] ATLAS Collaboration, *Improved luminosity determination in pp collisions at sqrt(s) = 7 TeV using the ATLAS detector at the LHC*, arXiv:1302.4393 [hep-ex].

[41] CMS Collaboration, *The CMS experiment at the CERN LHC*, JINST **3** (2008) S08004.

[42] CMS Collaboration, *Search for physics beyond the standard model in events with tau leptons, jets, and large transverse momentum imbalance in pp collisions at sqrt(s) = 7 TeV*, arXiv:1301.3792 [hep-ex].

[43] ATLAS Collaboration, *The ATLAS Experiment at the CERN Large Hadron Collider*, JINST **3** (2008) S08003.

[44] M. L. Mangano et al., *ALPGEN, a generator for hard multiparton processes in hadronic collisions*, JHEP **0307** (2003) 001.

[45] J. Pumplin et al., *New generation of parton distributions with uncertainties from global QCD analysis*, JHEP **0207** (2002) 012.

[46] T. Gleisberg et al., *Event generation with SHERPA 1.1*, JHEP **0902** (2009) 007.

[47] S. Frixione and B. R. Webber, *Matching NLO QCD computations and parton shower simulations*, JHEP **0206** (2002) 029.

[48] S. Frixione, P. Nason, and B. R. Webber, *Matching NLO QCD and parton showers in heavy flavor production*, JHEP **0308** (2003) 007.

[49] S. Frixione, E. Laenen, P. Motylinski, and B. R. Webber, *Single-top production in MC@NLO*, JHEP **0603** (2006) 092.

[50] B. Kersevan and E. Richter-Was, *The Monte Carlo event generator AcerMC version 1.0 with interfaces to PYTHIA 6.2 and HERWIG 6.3*, Comput. Phys. Commun. **149** (2003) 142–194.

[51] H. L. Lai et al., *New parton distributions for collider physics*, Phys.Rev. **D82** (2010) 074024.

[52] G. Corcella et al., *HERWIG 6: An Event generator for hadron emission reactions with interfering gluons (including supersymmetric processes)*, JHEP **0101** (2001) 010.

[53] J. Butterworth, J. R. Forshaw, and M. Seymour, *Multiparton interactions in photoproduction at HERA*, Z.Phys. **C72** (1996) 637.

[54] S. Jadach, Z. Was, R. Decker, and J. H. Kuhn, *The Tau Decay Library TAUOLA, Version 2.4*, Comput. Phys. Commun. **76** (1993) 361.

[55] P. Golonka et al., *The Tauola-Photos-F Environment for the TAUOLA and PHOTOS Packages, Release II*, Comput. Phys. Commun. **174** (2006) 818.

[56] E. Barberio and Z. Was, *PHOTOS - a Universal Monte Carlo for QED Radiative Corrections: Version 2.0*, Comput. Phys. Commun. **79** (1994) 291.

[57] T. Sjostrand, S. Mrenna, and P. Skands, *A Brief Introduction to PYTHIA 8.1*, Comput. Phys. Commun. **178** (2008) 852–867.

[58] ATLAS Collaboration, *ATLAS Tunes for PYTHIA6 and PYTHIA8 for MC11*, ATLAS-PHYS-PUB-2011-009, July, 2011. http://cdsweb.cern.ch/record/1363300.

[59] A. Sherstnev and R. S. Thorne, *Parton Distributions for LO Generators*, Eur. Phys. J. **C55** (2008) 553.

[60] S. Catani et al., *Vector boson production at hadron colliders: A Fully exclusive QCD calculation at NNLO*, Phys. Rev. Lett **103** (2009) 082001.

[61] A. Martin, W. Stirling, R. Thorne, and G. Watt, *Parton distributions for the LHC*, Eur.Phys.J. **C63** (2009) 189–285.

[62] M. Aliev, H. Lacker, U. Langenfeld, S. Moch, P. Uwer, et al., *HATHOR: HAdronic Top and Heavy quarks crOss section calculatoR*, Comput. Phys. Commun. **182** (2011) 1034–1046.

[63] J. M. Campbell, R. K. Ellis, and C. Williams, *Vector boson pair production at the LHC*, JHEP **107** (2011) 018.

[64] W. Porod, *SPheno, a program for calculating supersymmetric spectra, SUSY particle decays and SUSY particle production at e+ e- colliders*, Comput.Phys.Commun. **153** (2003) 275–315, arXiv:hep-ph/0301101 [hep-ph].

[65] W. Porod and F. Staub, *SPheno 3.1: Extensions including flavour, CP-phases and models beyond the MSSM*, Comput.Phys.Commun. **183** (2012) 2458–2469, arXiv:1104.1573 [hep-ph].

[66] M. Muhlleitner, A. Djouadi, and Y. Mambrini, *SDECAY: A Fortran code for the decays of the supersymmetric particles in the MSSM*, Comput. Phys. Commun. **168** (2005) 46–70.

[67] A. Djouadi, J. Kalinowski, and M. Spira, *HDECAY: A Program for Higgs boson decays in the standard model and its supersymmetric extension*, Comput. Phys. Commun. **108** (1998) 56–74.

[68] A. Djouadi, M. Muhlleitner, and M. Spira, *Decays of supersymmetric particles: The Program SUSY-HIT (SUspect-SdecaY-Hdecay-InTerface)*, Acta Phys. Polon. **B38** (2007) 635–644.

[69] B. Allanach, *SOFTSUSY: a program for calculating supersymmetric spectra*, Comput.Phys.Commun. **143** (2002) 305–331, arXiv:hep-ph/0104145 [hep-ph].

[70] M. Bähr et al., *Herwig++ Physics and Manual*, Eur. Phys. J. **C58** (2008) 639–707.

[71] W. Beenakker, R. Hopker, M. Spira, and P. Zerwas, *Squark and Gluino Production at Hadron Colliders*, Nucl. Phys. **B492** (1997) 51.

[72] A. Kulesza and L. Motyka, *Threshold resummation for squark-antisquark and gluino-pair production at the LHC*, Phys. Rev. Lett. **102** (2009) 111802.

[73] A. Kulesza and L. Motyka, *Soft gluon resummation for the production of gluino-gluino and squark-antisquark pairs at the LHC*, Phys.Rev. **D80** (2009) 095004.

[74] W. Beenakker et al., *Soft-gluon resummation for squark and gluino hadroproduction*, JHEP **0912** (2009) 041.

[75] W. Beenakker et al., *Squark and gluino hadroproduction*, Int. J. Mod. Phys. **A26** (2011) 2637–2664.

[76] M. Krämer et al., *Supersymmetry production cross sections in pp collisions at* $\sqrt{s} = 7\,TeV$, arXiv:1206.2892 [hep-ph].

[77] GEANT4 Collaboration, S. Agostinelli et al., GEANT4*: A simulation toolkit*, Nucl. Instrum. Meth. **A506** (2003) 250.

[78] ATLAS Collaboration, *The ATLAS Simulation Infrastructure*, Eur. Phys. J. **C70** (2010) 823.

[79] M. Cacciari, G. P. Salam, and G. Soyez, *The anti-kt jet clustering algorithm*, JHEP **0804** (2008) 063.

[80] ATLAS Collaboration, *Jet Energy Measurement with the ATLAS Detector in pp Collisions at* $\sqrt{s} = 7$ *TeV*, Eur. Phys. J. **C73** (2013) 2304.

[81] ATLAS Collaboration, *Muon reconstruction efficiency in reprocessed 2010 LHC proton-proton collision data recorded with the ATLAS detector*, Atlas-conf-2011-063, Apr, 2011. http://cdsweb.cern.ch/record/1345743.

[82] ATLAS Collaboration, *A measurement of the ATLAS muon reconstruction and trigger efficiency using J/psi decays*, Atlas-conf-2011-021, Mar, 2011. http://cdsweb.cern.ch/record/1336750.

[83] ATLAS Collaboration, ATLAS Collaboration, *Electron performance measurements with the ATLAS detector using the 2010 LHC proton-proton collision data*, Eur. Phys. J. **C72** (2012) 1909.

[84] ATLAS Collaboration, *Performance of the Reconstruction and Identification of Hadronic Tau Decays with ATLAS*, ATLAS-CONF-2011-152, Nov, 2011. http://cdsweb.cern.ch/record/1398195.

[85] ATLAS Collaboration, *Performance of Missing Transverse Momentum Reconstruction in Proton-Proton Collisions at 7 TeV with ATLAS*, Eur. Phys. J. **C72** (2012) 1844.

[86] ATLAS Collaboration, *Commissioning of the ATLAS high-performance b-tagging algorithms in the 7 TeV collision data*, ATLAS-CONF-2011-102, Jul, 2011. http://cdsweb.cern.ch/record/1369219.

[87] ATLAS Collaboration, *Measurement of the b-tag Efficiency in a Sample of Jets Containing Muons with 5* fb^{-1} *of Data from the ATLAS Detector*, ATLAS-CONF-2012-043, Mar, 2012. http://cdsweb.cern.ch/record/1435197.

[88] ATLAS Collaboration, *Performance of primary vertex reconstruction in proton-proton collisions at* $\sqrt{s} = 7$ *TeV in the ATLAS Experiment*, ATLAS-CONF-2010-069, 2010. http://cdsweb.cern.ch/record/1281344.

[89] G. Cowan, K. Cranmer, E. Gross, and O. Vitells, *Asymptotic formulae for likelihood-based tests of new physics*, Eur. Phys. J. **C 71** (2011) 1554.

[90] A. L. Read, *Presentation of search results: The* CL_s *technique*, J. Phys. **G28** (2002) 2693.

APPENDIX A

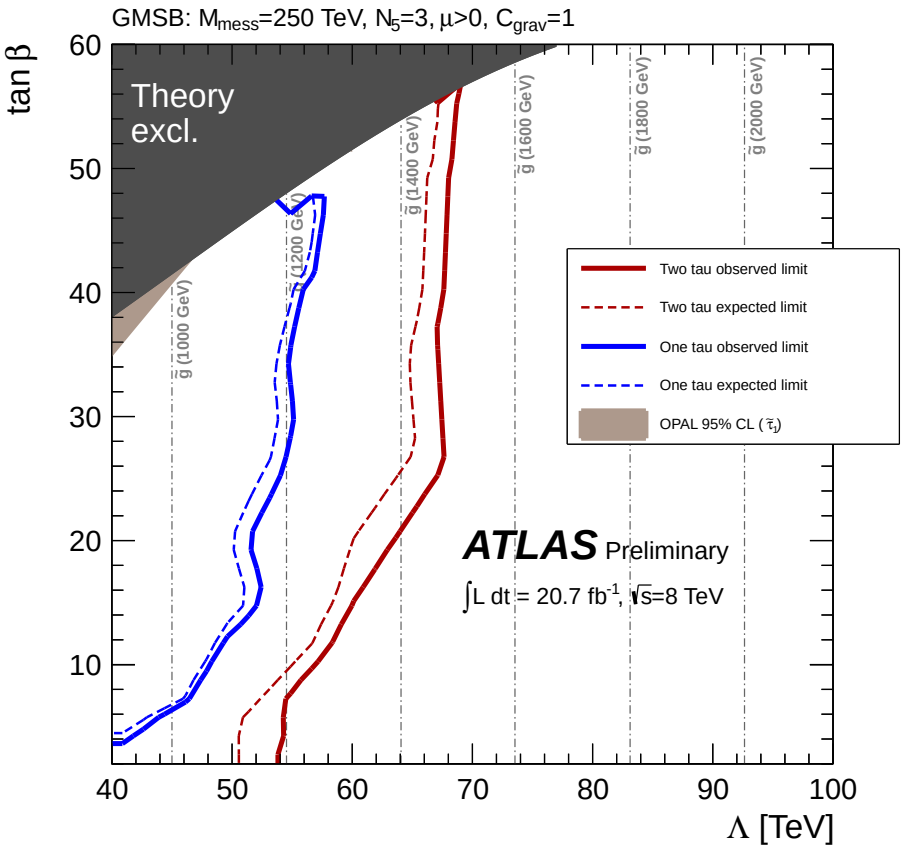

FIG. 1. Expected and observed 95 % CL lower limits on the minimal GMSB model parameters Λ and $\tan\beta$ for the 1τ and the 2τ analysis individually. The result is obtained using $(20.7 \pm 0.8)\,\mathrm{fb}^{-1}$ of proton-proton collision data at $\sqrt{s} = 8$ TeV recorded with the ATLAS detector at the Large Hadron Collider. The dark grey area indicates the region which is theoretically excluded due to unphysical sparticle mass values. Additional model parameters are $M_{\mathrm{mess}} = 250\,\mathrm{TeV}$, $N_5 = 3$, $\mu > 0$ and $C_{\mathrm{grav}} = 1$.